Title: Injury-Free In Vivo Delivery and Engraftment into the Cornea Endothelium Using Extracellular Matrix Shrink-Wrapped Cells

Authors: Rachelle N. Palchesko[1]*, Yiqin Du[2], Moira L. Geary[2], Santiago Carrasquilla[1], Daniel J. Shiwarski[1], Irona Khandaker[2], James L. Funderburgh[2], Adam W. Feinberg[1,3*]

Affiliations:

[1]Department of Biomedical Engineering, Carnegie Mellon University, 5000 Forbes Avenue, Pittsburgh PA, 15213.

[2]Department of Ophthalmology, University of Pittsburgh, 203 Lothrop Street, Pittsburgh PA, 15213.

[3]Department of Materials Science & Engineering, Carnegie Mellon University, 5000 Forbes Avenue, Pittsburgh PA, 15213.

*To whom correspondence should be addressed: rachelle@andrew.cmu.edu (R.P.); feinberg@andrew.cmu.edu (A.W.F.)

†Additional author notes should be indicated with symbols (for example, for current addresses).

One Sentence Summary: Small monolayers of interconnected endothelial cells are shrink-wrapped in a thin layer of ECM and exhibit enhanced adhesion and integration in vivo compared to single cell suspensions.

Abstract: Cell injection has emerged as a widespread approach for therapeutic delivery of healthy cells into diseased and damaged tissues to achieve regeneration. However, cell retention, viability and integration at the injection site has generally been poor, driving the need for improved approaches. Additionally, it is unknown how efficiently single cells can integrate and repair tissue level function. Here we have developed a technique to address these issues by engineering islands of interconnected cells on ECM nanoscaffolds that can be non-destructively released from the surface via thermal dissolution of the underlying thermo-responsive polymer. Upon dissolution of the polymer, the ECM nanoscaffold shrink-wraps around the small island of cells, creating a small patch of cells that maintain their cell-cell junctions and cytoskeletal structure throughout collection, centrifugation and injection that we have termed μMonolayers. These μMonolayers were made with corneal endothelial cells, as a model system, as single cell injections of corneal endothelial cells have been used with some success clinically to treat corneal blindness. In vitro our μMonolayers exhibited increased integration compared to single cells into low density corneal endothelial monolayers and in vivo into the high-density healthy rabbit corneal endothelium. These results indicate that this technique could be used to increase the integration of healthy cells into existing tissues to treat not only corneal blindness, but also other conditions such as cystic fibrosis, myocardial infarction, diabetes, etc.

Introduction

Organ and tissue transplants are the only option for patients with end-stage organ failure, and while effective, it is estimated by the World Health Organization that over 1 million people are unable to benefit due to global donor shortages. Patients must also remain on immunosuppressants for life with major side-effects, experience a high rate of organ failure and rejection, and have no access to transplantation in many parts of the world (*2*). As an alternative, cell-based therapies have long been thought of as a potential therapeutic option for a range of diseases and injuries caused by tissue and organ failure such as myocardial infarction (*3*), diabetes (*4*, *5*), corneal blindness (*6*), cystic fibrosis (*7*, *8*). The goal is to deliver viable cells that integrate into the target tissue and replace damaged or dysfunctional cells in order to stop or reverse disease progression. Potential advantages compared to transplant include minimally-invasive cell delivery without the need for extensive surgery, use of autologous cells to avoid immune rejection, and the ability to improve tissue and organ functional earlier in the disease process and thus entirely avoiding end-stage failure. Indeed, the past decade has seen advances in research and development of cell-based therapies based on autologous adult stem cells and induced pluripotent stem (iPS) cells (*9–11*). However, simple injection of cells into tissues has shown only limited clinical success in many applications due to low cell viability after injection as well as poor retention at the injection site and engraftment into the damaged tissue (*10*, *12*, *13*). Thus, there remains critical need for new technologies that can improve cell delivery, engraftment and function.

The cornea serves as a clinically relevant tissue for development of new cell delivery approaches because at >50,000 procedures annually in the US, it is transplanted more than all other solid organs combined (*14*). Specifically, we are focused on the corneal endothelium (CE),

a single layer of cells that lines the posterior surface of the cornea and is responsible for maintaining proper corneal thickness and clarity through regulation of stroma hydration. Nearly 50% of all corneal transplants are due to failure of the CE, primarily due to loss of CE cells that are cell cycle arrested and cannot replicate to repair damage or injury (*15–18*). This subsequently leads to failure to properly pump fluid from the stroma to the aqueous humor once the cell density drops below ~500 cells/mm^2, resulting in corneal edema (*19*, *20*). Current clinical treatment for CE failure is full thickness penetrating keratoplasty (PK) or partial-thickness transplants such as Descemet membrane endothelial keratoplasty (DMEK) and Descemet stripping automated endothelial keratoplasty (DSAEK) (*14*, *21*). These lamellar techniques have shown improvement over PK, with evidence that immune rejection is reduced with less stroma and extracellular matrix (ECM) transplanted (*22*, *23*). Further, the eye is considered to be immune privileged and eye drops are usually adequate rather than systemic immunosuppression. However, chronic rejection and limited donor supply in many parts of the world have motivated the development of new methods to inject CE cells into the anterior chamber to repopulate the endothelium and restore function (*6*). The problem these cell therapies have faced in the eye is the same as in other tissues and organs, effective delivery, and engraftment (*10*, *12*, *13*). In fact, most approaches require the existing CE to be removed through scrapping or cryogenic injury of the cornea in order to provide a place for the delivered cells to attach (*6*).

Here we report development of a new cell delivery method designed to enhance cell attachment and engraftment into tissues in vivo without requiring any induced damage to achieve integration. The challenge to delivering cells to the CE, and to epithelial and endothelial layers in general, is that these tissues are characterized by robust cell-cell injunctions and in general have evolved to act as barrier to keep things out. Thus, it has proved challenging to deliver single cells

in suspension, which do not have a mechanism to attach and integrate. To address this, we hypothesized that small patches of CE with intact tight junctions and cytoskeletal structure may exhibit improved adhesion and integration into existing CE monolayers compared to single cells. Specifically, our goal was to create a method where we could deliver viable cells to intact CE monolayers without removal of any cells and achieve integration that would increase cell density. To do this we developed an approach to shrink-wrap micron-scale monolayers (μMonolayers) of CE cells within a engineered layer ECM using an adaptation of our previous reported surface-initiated assembly technique (*24*, *25*). This technology enables the cells within the μMonolayers to maintain viability, tight-junctions and cytoskeletal structure throughout the release and injection process. Most importantly, the μMonolayers are able to integrate into existing CE monolayers and significantly increased cell density in both in vitro and in vivo assays. These results suggest that this technique could be used to increase cell density to treat corneal blindness without requiring the removal of the existing CE and enhance the engraftment of injected cells.

Results

Shrink-wrapped CE cells μMonolayers maintain cytoskeletal structure, tight junctions and high viability

To engineer the CE cell μMonolayers, bovine or rabbit CE cells were seeded onto micropatterned 200 x 200 μm squares of ECM proteins (1:1 laminin and collagen IV) (**Supplemental Fig. 1**) that were fabricated via surface-initiated assembly on thermo-responsive poly(n-isopropylacrylamide) (PIPAAm) substrates (**Fig 1.)**. The cells were cultured on the scaffolds for 24 hours to allow the cells to adhere to the scaffold, establish cytoskeletal structure and tight junctions, and form a confluent layer on each ECM square. Upon thermally-triggered

dissolution of the PIPAAm, the ECM square releases from the surface and effectively shrink-wraps around the CE cells forming the µMonolayer. Due to inherent pre-stress in the CE cells from being spread on the PIPAAm surface, once released the µMonolayers contract in size and are small enough to be injected through a small gauge needle.

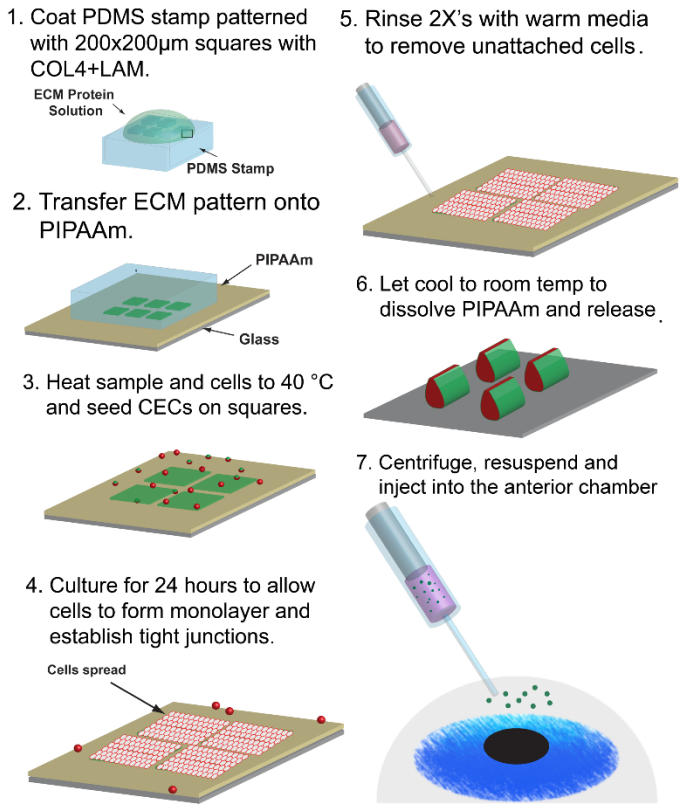

Fig. 1. Schematic representation of the process for shrink-wrapping and injecting corneal endothelial cell µMonolayers. Steps 1&2: Surface initiated assembly techniques are used to engineer 200 µm x 200 µm X 5 nm ECM scaffolds on the thermoresponsive polymer, PIPAAm. Steps 3&4: The samples and cells are then heated to 40 °C before seeding the cells on the squares and culturing for 24 hours. Steps 5&6: After 24 hours, samples are rinsed with warm media and cooled to room temperature to trigger the dissolution of the PIPAAm and shrink-wrapping/release of the µMonolayers of corneal endothelial cells before injection into the anterior chamber of the eye (Step 7).

To create the µMonolayers we needed to ensure that the CE cells would adhere and spread on the ECM squares to form confluent patches and then properly shrink-wrap. As a control, bovine CE cells were seeded onto ECM squares micropatterned onto polydimethylsiloxane (PDMS) substrates because it is not temperature sensitive and previous

studies have established cell growth on this surface (*25–29*). After 24 hours, the CE cells on the ECM squares on PDMS were adhered and spread into a monolayer as expected (**Fig. 2A**). Next, we repeated this by seeding CE cells on ECM squares patterned on PIPAAm, and the cells exhibited a similar morphology when viewed under phase microscopy (**Fig. 2B**). Upon dissolution of the PIPAAm and thermal release, the cells remained interconnected and were successfully shrink-wrapped within the ECM squares into µMonolayers (**Fig. 2C**). Time-lapse images show that once the media reached room temperature and the PIPAAm dissolved (0 sec), the shrink-wrapping process occurred quickly in <100 seconds (**Fig. 2D, Supplemental video S1**).

After release, the shrink-wrapped µMonolayers were collected, centrifuged, injected through a 28G needle onto a glass coverslip and allowed to settle for 30 min before fixing and staining to investigate the morphology, structure, and viability of the CE cells. The shrink-wrapped CE cells exhibited continuous ZO-1 at the borders and a cortical F-actin structure indicating that the cells maintained their tight-junctions and cytoskeletal structure throughout the release and injection process (**Fig. 2E**). Immediately post-release, the shrink-wrapped µMonolayers contracted tightly into small clusters (**Fig. 2C**), however, approximately 30 minutes after release and injection the µMonolayers relaxed and returned to a disc-like morphology as they settled onto the surface (**Fig. 2F**). This establishes that the shrink-wrapping process and subsequent injection through a small gauge needle does not disrupt cell-cell adhesions or cause damage to the CE cells in the µMonolayer. High cell viability in the µMonolayers after injection was confirmed using a Live/Dead cytotoxicity assay and compared to enzymatically-released single cells (**Fig. 2G**). Confocal microscopy images revealed that the only dead cells were those that were not integrated into the shrink-wrapped µMonolayers, with

cells in the µMonolayers showing very high viability (**Fig. 2G**, shown by the arrows). Quantitative image analysis showed that single CE cells in suspension had 93 ± 4% viability and the CE cells within the shrink-wrapped µMonolayers had 97 ± 2% viability, though this difference was not statistically significant (**Fig. 2H).**

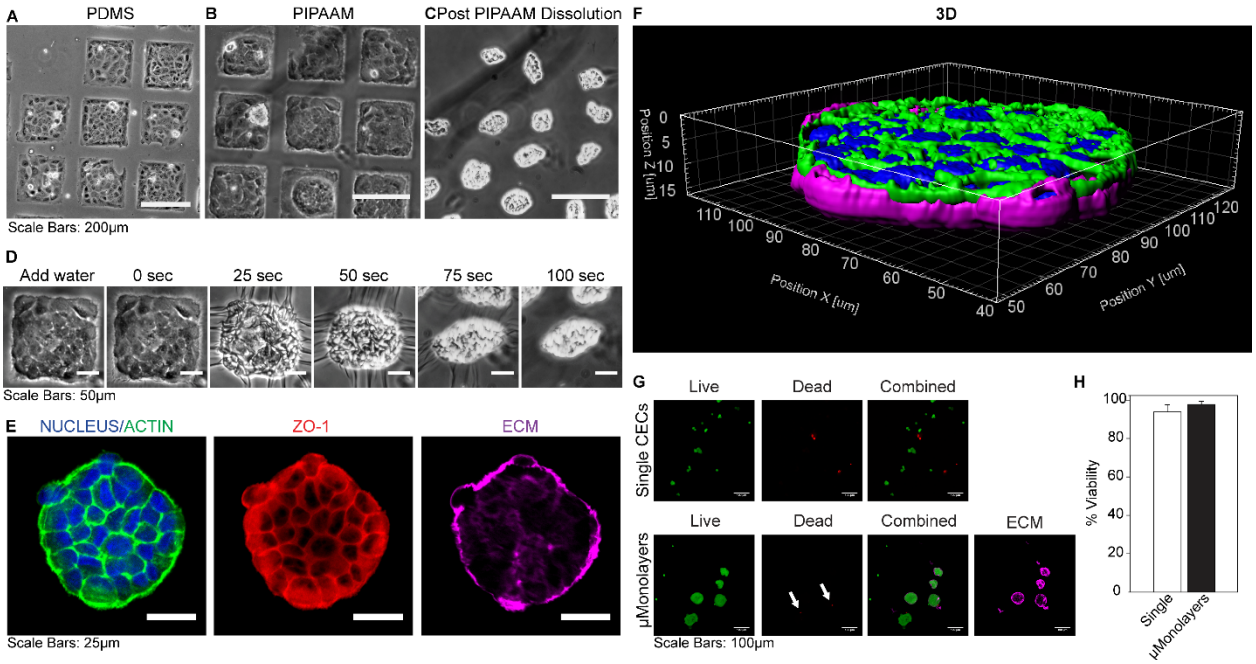

Fig. 2. CE cells form µMonolayers on ECM squares and maintain their structure and viability through shrink-wrapping and injection. (A) CE cells form monolayers on ECM squares microcontact printed onto PDMS (used as a control) and **(B)** on the thermoresponsive polymer PIPAAm. **(C)** Once the PIPAAm is dissolved the CE CELL µMonolayers contract and are shrink-wrapped in the ECM squares. **(D)** The release and shrink-wrapping of µMonolayers occurs quickly, in <100 seconds once the water + sample cools to room temperature. **(E)** Confocal microscopy images show that after injection, the CE cells maintain both their cytoskeletal structure (F-actin, green), tight junctions (ZO-1, red) and adherence to the ECM scaffold (LAM+COL4, purple). **(F)** A 3D projection of a shrink-wrapped CE CELL µMonolayer 30 minutes after injection onto a glass surface illustrating how it begins to relax and return to its original shape. **(G)** Representative live/dead images of control single CE cells and shrink-wrapped CE cells show that both types of cells are viable with very few dead cells present. **(H)** Live/dead data showed no significant difference in viability between single cells (93 ± 4 %) and shrink-wrapped cells (97 ± 2 %) following injection through a 28G needle (n=3; mean ± stdev.; N.S. by Student's t-test Single vs. µMonolayers).

Shrink-wrapped µMonolayers rapidly adhere and spread to form a CE monolayer on collagen gels in vitro

To assess the potential of the shrink-wrapped µMonolayers for cell injection therapy, we first performed an in vitro assay using a compressed collagen type I gel as a model of a denuded

corneal stroma. Shrink-wrapped μMonolayers and single CE cells in suspension (as the control) were seeded onto compressed collagen type I gels by injecting through a 30 gauge needle. Samples were fixed and stained post-injection at 6 hours to observe initial attachment and adhesion and at 24 hours to observe and spreading and outgrowth. At 6 hours post-injection, single CE cells were mostly rounded with very little spreading observed (**Fig. 3A**) and the F-actin staining showed a lack of filamentous cytoskeleton structure, additionally there was no ZO-1 observed. In contrast, the CE cells from the shrink-wrapped μMonolayers maintained their cytoskeletal structure and tight-junctions, as evidenced by the F-actin filaments and continuous ZO-1 expression at the cell borders (**Fig. 3B**). Examining the samples in 3D confirmed that single CE cells were rounded and had few contacts between cells (**Fig. 3A**) whereas the shrink-wrapped μMonolayers had reoriented with cells directly attached to the collagen and the ECM scaffolds now present within the center of the monolayer (**Fig. 3B**). After 24 hours, the single CE cells covered most of the collagen substrate and had a more defined cytoskeletal structure (**Fig. 3C**) but with many F-actin stress fibers across the cell bodies rather than being primarily cortical. Additionally, the single CE cells exhibited very low ZO-1 staining, expressed discontinuously at the cell borders (**Fig. 3C**). In contrast, the shrink-wrapped μMonolayers had continuous ZO-1 at all cell borders and abundant cortical F-actin (**Fig. 3D**), which closely resembled the structure of in vivo CE cells (*30*). The remnants of the ECM squares were still visible after 24 hours as indicated by the arrows in **Fig. 3D**. These results show that CE cells in shrink-wrapped μMonolayers have comparable or better ability as CE cells in suspension to repopulate a collagen substrate.

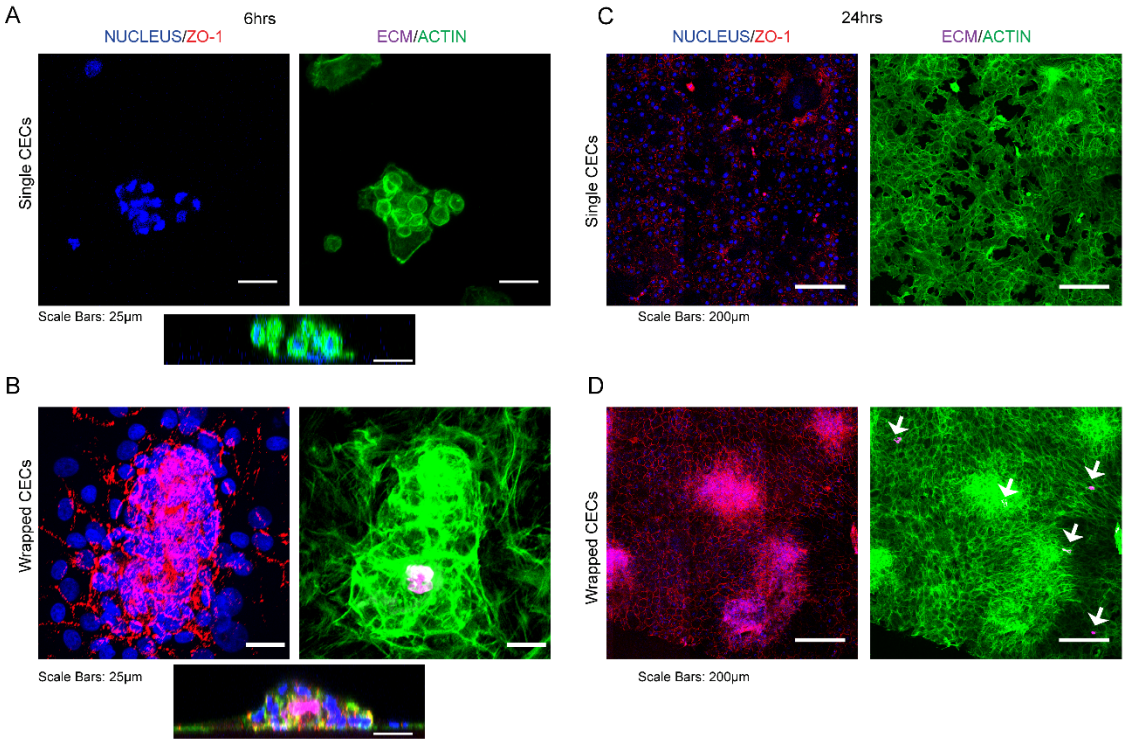

Fig. 3. Shrink-wrapped CE CELL μMonolayers maintain ZO-1 expression F-actin cytoskeleton as they grow out of the ECM scaffolds to form a monolayer on a collagen I stromal mimic. (A) Six hours after reseeding onto a collagen I gel, the single CE cells have no established F-actin cytoskeleton or ZO-1 expression. In contrast, the CE cells in the shrink-wrapped μMonolayers have maintained their ZO-1 expression and F-actin cytoskeleton, while growing out of the ECM scaffolds. The cells at the periphery of the shrink-wrapped CE cells are also expressing ZO-1. **(B)** The 3D views of the cells at 6 hours post-seeding show the differences between the single CE cells and shrink-wrapped CE cells. Images on the left are cross-sectional projections of the 3D views. **(C)** At 24 hours, single CE cells have begun to spread and cover almost the entire scaffold. **(D)** At 24 hours, the CE cells have already grown out of the ECM scaffolds and formed an almost complete monolayer. For A-D: Nucleus = blue, ZO-1 = red, ECM(COL4) = magenta, F-actin =green.

Shrink-wrapped μMonolayers show enhanced engraftment into existing CE monolayers and increase CE density in vitro

Current clinical trials to restore the CE require removal of the existing CE cells in order to make space to deliver the new cells and allow them to attach. This is because cells seeded onto an existing endothelial or epithelial layer typically show very low attachment and engraftment. Rather than damaging a tissue in order to repair it, we hypothesized that the shrink-wrapped μMonolayers would be able to engraftment into existing CE monolayers through enhanced cell-

cell and cell-ECM binding. To test this, we seeded shrink-wrapped CE cell μMonolayers in vitro onto an existing CE monolayer engineered to have lower density to mimic that observed in patients that need a cornea transplant. The CE cells were labeled with CellTracker green and used to form μMonolayers or as a single cell suspension control and injected through a 30G needle to seed them. CE monolayers that were not seeded with any cells served as negative controls. The seeded CE cells and μMonolayers were allowed to settle onto the samples for 3 hours before rinsing and adding fresh media. This process mimics the clinical procedure used for current CE cell injection in animal models and in human patients, where they remain face down for 3 hours post-injection (*6*, *31*, *32*). Samples were then cultured for 3, 7 and 14 days post-injection and analyzed for engraftment (**Fig. 4A**). At each time point, very few of the seeded single CE cells were integrated into the existing CE monolayers, and typically large areas of the samples had to be imaged to find labeled cells. In contrast, at day 3, the shrink-wrapped μMonolayers were well integrated across the samples and appeared as more densely packed compared to the CE cells existing monolayer. At day 7, the shrink-wrapped CE cells in the μMonolayers had completely integrated into the existing CE monolayer. The CellTracker positive CE cells from the μMonolayers still appeared to be more densely packed than those from the existing monolayer but were more spread out (**Fig. 4A**). By day 14, the CE cells from the shrink-wrapped μMonolayers appeared to be well engrafted and of similar density to the surrounding CE cells from the existing monolayer. By this time point it appeared that the density of the engrafted cells had equilibrated with the CE cells in the existing monolayer, achieving a new and increased overall cell density.

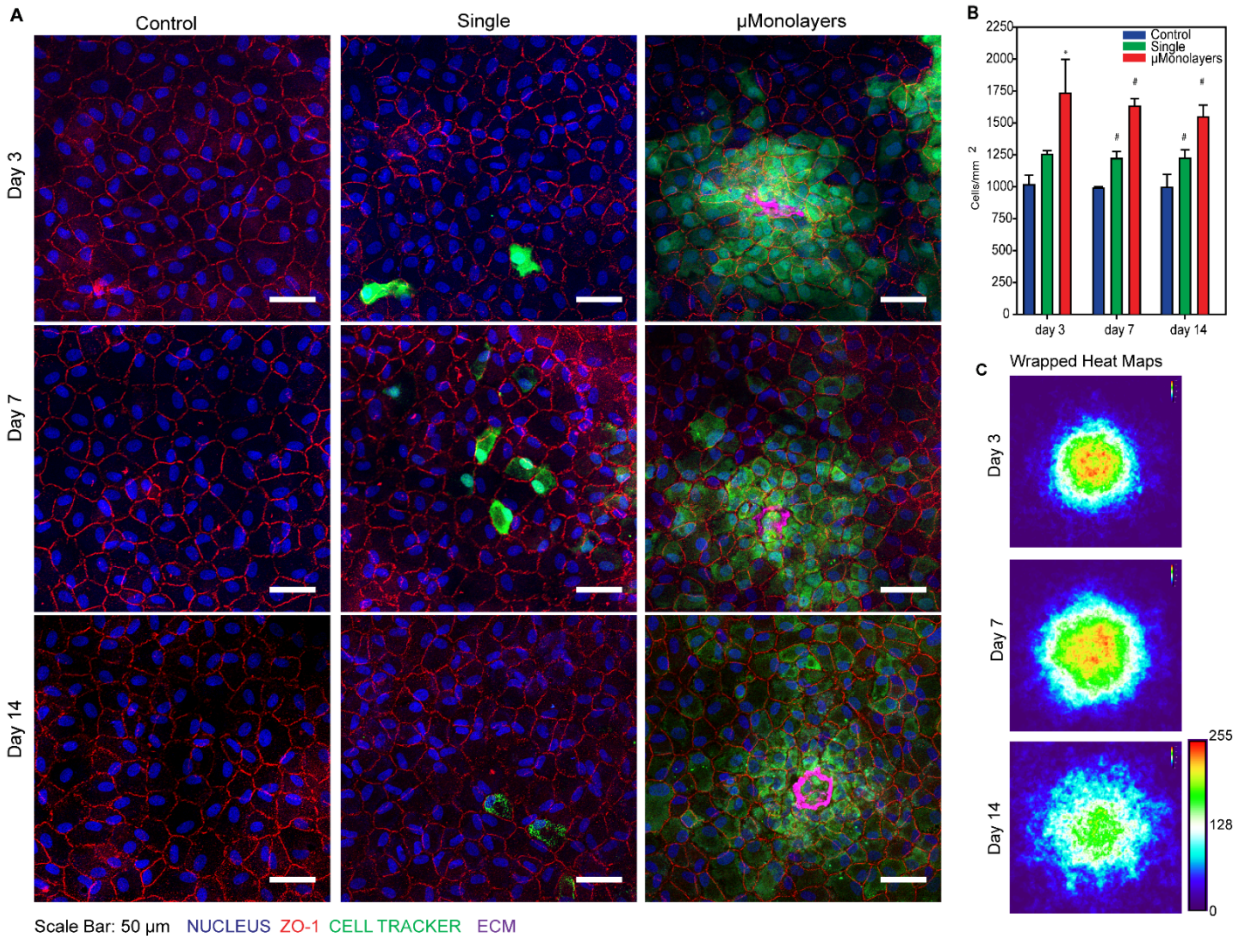

Fig. 4. Injected shrink-wrapped µMonolayers integrate into existing monolayers of CE cells and significantly increase the density compared to single CE cells. (A) Cell Tracker labeled single cells and shrink-wrapped cells were visible at all time points however, significantly more shrink-wrapped cells were present at all time points and the ECM scaffolds were still visible 14 days after injection. Scale bars = 50 µm. **(B)** The cell density of the monolayers was calculated and compared at days 3, 7 and 14. Data is represented as mean ± std dev. Day 3: Control = 1016 ± 75 cells/mm^2; Single = 1253 ± 31 cells/mm^2 ; µMonolayer = 1731 ± 267 cells/mm^2. Day 7: Control = 989 ± 11 cells/mm^2 ; Single = 1220 ± 56 cells/mm^2; µMonolayer = 1631 ± 58 cells/mm^2. Day 14: Control = 994 ± 104 cells/mm^2; Single = 1224 ± 66 cells/mm^2; µMonolayer = 1545 ± 95 cells/mm^2.The data was compared using a one-way ANOVA on ranks with Tukey's test (day 3) or one-way ANOVA (day 7 and 14) with Tukey's Test is SigmaPlot. * = statistically significantly different from control, # = statistically significantly different from all other samples. Day 3: n=4 for all samples; Day 7: control n=3, single n=4, wrapped n=4; Day 14: control n=4, single n=3, wrapped n=4. **(C)** Heat maps of Cell Tracker positive pixels show that the cells in the shrink-wrapped µMonolayers initially integrate into a tight cluster and then the density equilibrates as the cells spread out slightly (Day 3 n= 33, Day 7 n= 37, Day 14 n= 40, scale bar is arbitrary units).

To determine how well the shrink-wrapped CE cell µMonolayers engrafted and increased the cell density of the low-density CE monolayers, the density was analyzed at each time point. Overall, the single CE cells increased the monolayer density ~20% while the shrink-wrapped CE cell µMonolayers increased the monolayer density ~50%, even though the same total number of

cells were seeded for each condition (**Fig. 4B**). At day 3, the shrink-wrapped μMonolayers significantly increased cell density compared to controls and at days 7 and 14 the shrink-wrapped μMonolayers significantly increased cell density compared to both controls and samples seeded with single CE cells. These results establish that the shrink-wrapped μMonolayers adhere, engraft, and then spread out into an existing CE monolayer in a manner that single CE cells cannot. Further, we generated heat maps using images of the CellTracker green labeled CE cells in the shrink-wrapped μMonolayers to confirm that the cells were spreading out over time (**Fig. 4C**). The results confirm that at day 3 the CE cells are contained in a small area and that over time they spread out into the surrounding monolayer and equilibrate in density. This makes sense, because even though the images of fixed CE monolayers makes it look like the cells are stationary, time-lapse images routinely show that cells are constantly moving within epithelial layers (*33*, *34*), which should facilitate the spreading out of the shrink-wrapped CE cells. This continued equilibration also explains the perceived decrease in cell density from day 3 to 14, where the cell density overall isn't decreasing, it is just becoming more homogenous across the CE monolayer. This was confirmed by running a one-way ANOVA within each sample type comparing the densities over time, which showed that the time point had no statistically significant effect.

Shrink-wrapped μMonolayers rapidly flatten against and begin to integrate into the CE within 3 hours

Clinical injection of single CE cells requires that patients lie face down for 3 hours post injection to allow for cell attachment to the CE on the posterior of the cornea. Thus, a major question for the shrink-wrapped μMonolayers is how they achieve improved engraftment and

how long does it take compared to single cells. To address this, we performed live confocal imaging of the integration by labeling the shrink-wrapped μMonolayers with CellTracker™ Green and the cells in the low-density monolayer with CellTracker™ Orange. By collecting a Z-stack every hour for 48 hours, we were able to clearly observe the dynamics of the integration process from both top-down and side views (**Supplemental videos S2 and S3**). At 3 hours post-injection, the shrink-wrapped μMonolayers had begun to attach and flatten on top of the low-density monolayer (**Fig. 5A**). Over time the shrink-wrapped μMonolayers continued to flatten and move around as the cells moved into the underlying low-density monolayer. By 43 hours, the shrink-wrapped μMonolayer was almost completely integrated into the CE monolayer and appeared to be in the same imaging plane with the low-density monolayer and not sitting on top of it. The ECM square used in the shrink-wrapping process remained centrally located underneath the cell bodies of the shrink-wrapped cells, which is consistent with results from the fixed time point experiments (**Fig. 4A**).

Although the time-lapse imaging results suggested that 3 hours is sufficient for the shrink-wrapped μMonolayers to attach to the CE, potential differences between in vitro and in vivo conditions caused us to assess attachment to the native cornea. To do this, we switched to rabbit CE cells and injected shrink-wrapped μMonolayers ex vivo into the anterior chamber of enucleated rabbit eyes. The eyes were then incubated with the cornea facing down for 3 hours to allow attachment of the shrink-wrapped μMonolayers before fixation and staining of the whole globe (**Supplemental Fig. S2**). Confocal imaging of the corneas showed numerous shrink-wrapped μMonolayers attached over the entirety of the posterior surface (**Fig. 5B**). At this 3-hour time point, the shrink-wrapped μMonolayers were still disc-like in shape and oriented with the ECM layer facing the CE on the posterior surface of the cornea. This is consistent with the

observations from the time-lapse experiments. These experiments provided confidence that 3 hours was sufficient for gravitational settlement and attachment of the shrink-wrapped μMonolayers for subsequent in vivo experiments.

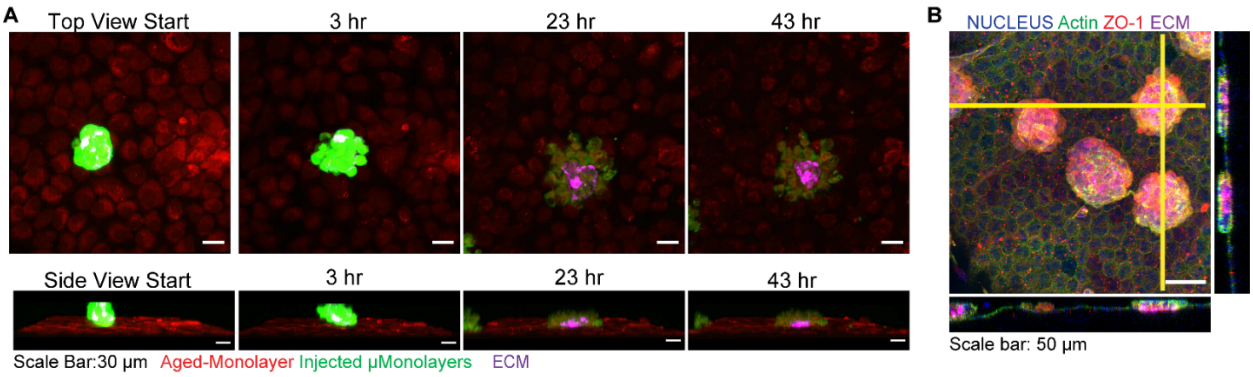

Fig. 5. Shrink-wrapped μMonolayers begin to integrate into "aged" CE monolayers and ex vivo corneas within 3 hours. (A) Time-lapse images from live confocal imaging of the integration of shrink-wrapped bovine μMonolayers (Cell Tracker green) into an engineered "aged" bovine CE monolayer (Cell Tracker Orange). At 3 hours, the μMonolayers have attached and begun to integrate and by 43 hours the cells are almost completely integrated into the monolayer. **(B)** Confocal images show that the shrink-wrapped μMonolayers had begun to integrate into the ex vivo rabbit CE and the ECM scaffold is observed to be between μMonolayers and the existing rabbit CE. The yellow vertical and horizontal lines indicate the places at which the orthogonal views were obtained.

Shrink-wrapped μMonolayers show robust engraft into the CE in vivo

Having demonstrated enhanced engraftment of the shrink-wrapped μMonolayers in vitro and ex vivo, we moved next to an in vivo rabbit model. First we assessed the basic feasibility of injecting the shrink-wrapped μMonolayers in vivo and achieving engraftment. To do this, shrink-wrapped μMonolayers (n=3) or single cells (n=2) were labeled with DiO and 100,000 cells in 50 μL of DMEM/F12 were injected into the anterior chamber of one eye for each rabbit. The rabbits were laid on their sides with the injected eye facing down for 3 hours to allow for cell attachment and integration and then followed daily for 7 days before sacrifice and enucleation. On day 7, the injected eyes on all 5 rabbits remained clear with no visible outward signs of irritation or swelling and appeared to be same as the contralateral control eye in each animal (**Fig. 6A,B,**

Supplemental Fig 3.). Additional examination by Confoscan indicated no abnormalities in the corneal endothelium (**Supplemental Fig 4**). These results establish that (i) the injection process to deliver shrink-wrapped µMonolayers to the anterior chamber does not damage the cornea, and (ii) that there is no immune response in terms of cell infiltration that would cloud the cornea due to the allogeneic rabbit CE cells.

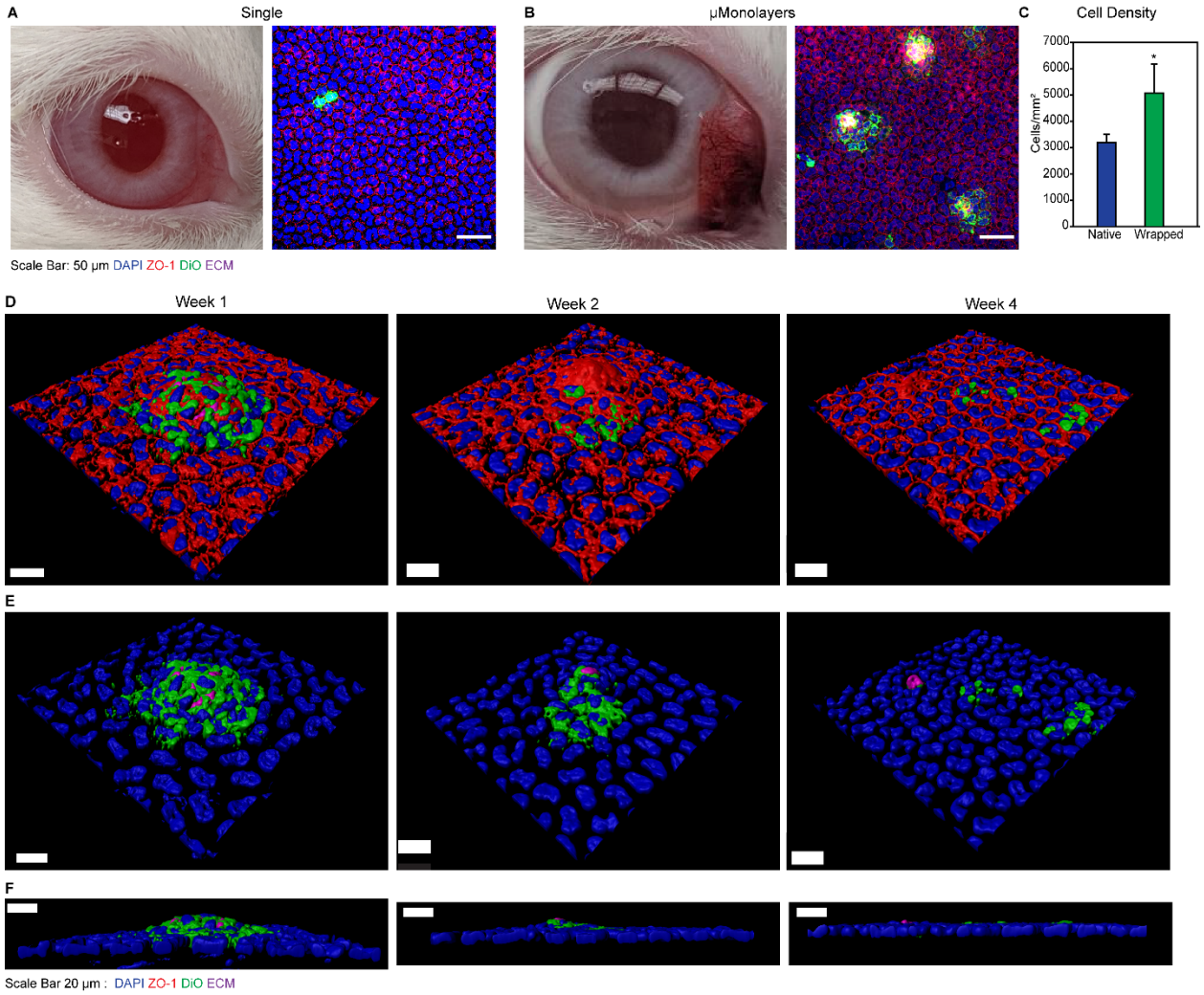

Fig. 6. Shrink-wrapped µMonolayers integrate into the existing healthy rabbit CE. (A) Rabbit corneas injected with single cells remained clear at 1-week post injection. However, very few DiO labeled single cells are observed integrated into the rabbit CE. **(B)** The rabbit cornea injected with µMonolayers also remained clear 1-week post injection and numerous clusters of µMonolayers were observed in each cornea with the continuous ZO-1 at the borders between DiO labeled cells and native rabbit CE cells. **(C)** Graph showing the cell density in the areas of the integrated shrink-wrapped µMonolayers (green bar) compared to native areas within the same image with no DiO labeled cells (blue bar). Data is represented as mean ± standard deviation and was compared using a student T-test. It was found that the density in the areas with shrink-wrapped µMonolayers was significantly higher than the native CE cell density (* $p<0.05$). **(D)** Confocal microscopy images showing the integrated DiO labeled shrink-wrapped µMonolayers at 1,

2- and 4-weeks post-injection. Nuclei = blue, DiO labeled cells (green), ZO-1 (red), ECM nanoscaffold (purple). **(E)** The same images from panel D with the ZO-1 removed to highlight the nuclei of both the healthy rabbit endothelium and injected cells (blue), DiO labeled injected rabbit cells (green) and ECM nanoscaffold (purple) from the shrink-wrapping process at 1, 2- and 4-weeks post-injection. **(F)** The orthogonal views of the confocal images shown in panel E showing the integration of the shrink-wrapped µMonolayers into the healthy rabbit endothelium over the 4 week period post-injection. Scale bars in D-F are 20 µm.

After enucleation, the eyes were fixed, and the corneas were stained as wholemounts for the tight junctions via ZO-1 and the nuclei to observe integration into the healthy rabbit CE. Confocal microscopy imaging showed that very few DiO labeled cells were present in the single cell injected eyes of both rabbits (**Fig. 6A and Supplemental Fig. 6A**) with only a few labeled cells being found across the entire cornea. In contrast, numerous clusters of shrink-wrapped µMonolayers integrated throughout the corneas of all 3 rabbits injected with the µMonolayers (**Fig. 6B and Supplemental Fig. 6B**). Cell density of the integrated µMonolayers was compared to control areas within the same cornea (example areas shown in **Supplemental Fig 5)** and results showed that the areas of shrink-wrapped µMonolayers had a significantly higher cell density compared to the areas without integrated shrink-wrapped µMonolayers (**Fig. 6C, *).** Higher magnification imaging showed that the cells of the shrink-wrapped µMonolayers had integrated with the healthy rabbit CE with ZO-1 present continuously at all cell borders between the DiO labeled cells and the native rabbit CE cells (**Fig. 6D**). Additionally, the ECM scaffolds were still visible, providing further evidence that the shrink-wrapped µMonolayers had integrated and become a part of the rabbit CE in vivo (**Fig. 6E**). The cell density around the shrink-wrapped µMonolayers was higher than that of the area surrounding it.

To determine if the shrink-wrapped µMonolayers remained stable over time and to see if the high-density areas began to spread across the cornea, a second in vivo experiment was performed with shrink-wrapped µMonolayers at 2 weeks (n=2) and weeks (n=3). Comparable to week 1, all eyes at weeks 2 and 4 had no visible signs of irritation or swelling (**Supplmental Fig**

3.) and Confoscan indicated no abnormalities in the corneal endothelium (**Supplemental Fig 4**). At each time point labeled CE cells and ECM squares were detected, indicating that the cells remained viable, and stably integrated. Further, the presence of the ZO-1 between the native and shrink-wrapped cells indicated that a continuous monolayer was established (**Fig 6D**). Interestingly, when the ZO-1 and F-actin channels are removed from the images, at week 1, the ECM appears to be at the center of the cell nuclei (**Fig. 6E**), but is also underneath of the cell bodies as the cells were not on top of the native CE cells and the continuous ZO-1 indicated the cells were integrated with the native cells. By weeks 2 and 4, the density of the nuclei tightly surrounding the ECM begins to decrease as the ECM also becomes smaller (**Fig 6E**). The orthogonal views in **Fig. 6F** further confirms that the ECM begins to become smaller, and eventually the ECM and shrink-wrapped μMonolayer cells are flush with the surrounding native CE. To quantify the cell density and degree of integration of the injected μMonolayers, cell density of images with green cells present were compared to the density of images where there were no green cells present. In this experiment the entire images were used as there is a possibility that the DiO fades with time, so therefore we cannot be certain that all injected cells are still fluorescing green. In both week 2 rabbits, there was no significant difference in the density of the areas with DiO labeled cells compared to areas with no labeled cells (**Supplemental Fig 7A**) and only one of the 4 week rabbits had a statistically significant difference in the cell density of areas with labeled cells (**Supplemental Fig 7B**). These results combined with the orthogonal views from the confocal imaging indicate that the density has begun to equilibrate across the entire CE and there are no longer very high density patches where the μMonolayers initially adhered to the healthy rabbit CE. These results are in agreement with the equilibration of the density across the monolayer that we observed in vitro. All of the in vivo

results combined indicate that shrink-wrapped μMonolayers are able to stably integrate into the rabbit corneal endothelium and remain viable long-term.

Discussion

Cell injection therapy has had limited translation into clinical applications because of the lack of cell viability, retention, and integration at the injection site (*10*, *12*, *13*). Many studies have shown that these types of interactions are crucial, particularly for endothelial cells, for functions such as activation of signaling pathways, formation of cytoskeletal structure and focal adhesions, growth, survival, and proliferation. However, in the literature, most methods investigated to improve the success cell injection therapy have focused on the use of stem cells as opposed to differentiated cells, or methods to increase either the retention or adhesion of the cells at the injection location such as hydrogels, small molecules in the injection media (such as the ROCK inhibitor Y-27632) pre-conditioning of cells on ECM proteins, or genetic modification (*6*, *32*, *35–37*). While these methods have shown some improvements, they still fail to address the lack of cytoskeletal structure, and cell-cell and cell-ECM interactions exhibited by single cells.

Specifically, previous work by the Kinoshita group on the culture and injection of CE cells has highlighted the significance of the actin cytoskeleton on the adhesion of CE cells in vivo. Their research has shown that enzymatic dissociation of cells induces the phosphorylation of myosin light chain (MLC) through the Rho/ROCK pathway, which induces actin contraction and this activation of MLC negatively regulates cell adhesion (*31*). To overcome this, they inject the ROCK inhibitor Y-27632 with the CE cells, which enhances cell adhesion by blocking the actin contraction, therefore increasing the interactions between the cytoskeleton and focal adhesion complexes and integrins (*32*). Cytoskeletal structure and tight-junctions are necessary

for corneal endothelial cell function, therefore, single cells may not be able to adhere to the existing monolayer and repair tissue level function of the damaged endothelial layer. We therefore hypothesized that (i) injected single cells have poor viability and attachment to intact tissues, due to their lack of cell-cell junctions, cell-ECM interactions and cytoskeletal structure and (ii) that monolayers of cells with dimensions small enough to be injected through a small gauge needle, would integrate into existing CE monolayers in higher numbers compared to single cells.

Our technology to shrink-wrap μMonolayers in a thin layer of ECM protein that allows cells to maintain high viability, cell-cell junctions, and cytoskeletal structure post-injection, while also providing the cells with important cell-ECM interactions and tested the ability of these μMonolayers to engraft into tissues using the corneal endothelium as a model system. Our in vitro results confirmed that the CE cells formed a monolayer on the engineered ECM substrates and within 24 hours had established tight junctions and formed an organized F-actin cytoskeletal structure, which was retained through the thermal release process and injection through a 30G needle. When compared to enzymatically released single cells, injected shrink-wrapped μMonolayers significantly increased CE monolayer cell density in vitro. Additionally, shrink-wrapped μMonolayers exhibited initial attachment to both engineered low density monolayers and ex vivo corneas within 3 hours, indicating our technology has great translational potential, as it could be easily applied using the protocols that are currently in use in clinical trials for single-cell CE injection.(*6*) Further, the μMonolayers were able to integrate into these tissues without the need to disrupt the cell-cell tight junctions or removal of the existing cells prior to seeding, which is the standard clinical practice for those patients with remaining CE cells.(*6*)

To further demonstrate the ability of the μMonolayers to integrate into existing tissues, in vivo rabbit studies were performed utilizing healthy rabbit eyes and results showed high numbers of shrink-wrapped μMonolayers integrated into the healthy CE and remained integrated over 4 weeks. This is extremely promising as cells within a young healthy rabbit CE are contact-inhibited, have tight-junctions, and are at an extremely high density. Therefore, if the shrink-wrapped μMonolayers can integrate within such a tissue, integration into damaged or diseased CEs with a much lower cell density would occur at much higher rates. This is all further evidence that injection of μMonolayers could be used for patients who are experiencing declines in cell density and visual acuity to boost their CE cell density before it reaches the lower limit where corneal blindness results, thus increasing the life-span of their existing cornea and eliminating the need for a future transplant.

While these results are extremely promising, the in vivo study was limited in that cell integration into a healthy high-density CE is most likely limited so we are unable to determine the upper limits of number of cells that can be integrated into an existing diseased tissue. Ideally, this technology would be tested in an in vivo CE model that is more representative of patients with a low cell density, our target population, however, such an in vivo model does not currently exist(*38*) and as the low density observed in humans is caused by decades of aging and exposure to UV light(*39*, *40*), we could not develop a model to effectively recapitulate the disease state we are ultimately aiming to treat. For these reasons, we chose the healthy rabbit in vivo model, as we determined it was more relevant than a complete injury and removal model that has been used in other rabbit CE studies. Finally, another limitation of this study is the variability in cell density from cornea to cornea, even within the same rabbit adds a layer of difficulty to quantifying any effect on cell density within the healthy CE model. However, the results from

our in vitro studies utilizing lower density CE monolayers showed a significant increase in cell density of >50% when μMonolayers were injected compared to single cell suspensions and this combined with the results from our two in vivo rabbit studies indicated that this method of shrink-wrapping μMonolayers in a thin layer of ECM can be used to increase the integration of cells at the intended injection site.

Future experiments will expand upon our proof-of-concept studies to include larger in vivo rabbit studies, in both healthy and fully stripped CE models to allow for more robust methods of quantification such as repopulated CE cell density of injected shrink-wrapped μMonolayer vs single cells in the fully stripped CE model. While these models are again not fully representative of a patient population with low cell density, the fully stripped CE model is representative of those patients needing a full CE replacement and like the cell injection studies done in animal models and in humans clinically in other groups, which will allow us to compare this technology more directly with those methods. In the future, we also hope to apply this technology to therapeutic applications in other target organs, such as the heart and liver that also suffer from shortage of donor organs and lack of successful cell injection therapies and for the treatment of genetic diseases such as Cystic Fibrosis where recent advances in gene-editing and induced pluripotent stem cell technologies, have opened up the possibility of patient specific cell-based therapies.

Materials and Methods:

Study Design:

The research objectives of this study were to: 1) modify our previously published SHELL technique that was used to shrink-wrap single cells in order to shrink-wrap small islands of

corneal endothelial cells, 2) to investigate whether shrink-wrapped μMonolayers would integrate into and increase monolayer cell density *in vitro* and 3) determine if the μMonolayers were capable of integrating into an existing healthy CE *in vivo.* Primary bovine and rabbit cells were used throughout the study using previously published cell culture methods with minor modifications in the case of the rabbit cells.(*30*, *32*) Sample sizes for in vitro studies were determined by using the minimum number of samples to be considered statistically significant and time points/end points were based on our previously published studies. For the in vitro cell density study, 4 replicates per sample type per time point were used and 1 full study was completed. Data from day 3 time point was used to determine if the sample size was sufficient enough to provide statistical significance. At day 7 one control sample and at day 14 one single cells sample was lost during fixing and staining and therefore the n=3 for those sample types. In vivo studies were designed to be pilot studies and as such the number of rabbits per study was kept to a minimum.

ECM scaffold fabrication:

The ECM scaffolds were fabricated via previously described surface-initiated assembly techniques with minor modifications.(*24*, *25*) Briefly, 1 cm x 1 cm PDMS stamps designed to have 200 μm x200 μm square features were fabricated via standard soft lithography techniques. The stamps were sonicated in 50% ethanol for 60 minutes, dried under a stream of nitrogen and incubated for 60 minutes with a 50:50 mixture of 50 μg/mL collagen IV (COL4) and 50 μg/mL laminin (LAM) (**Fig. 1 step 1**). Either 50% AlexaFluor 488 labeled COL4 or 50% AlexaFluor 633 labeled LAM (for a final concentration of 25% labeled protein) was used to visualize the pattern transfer. Following incubation the stamps were rinsed in sterile water, dried under a stream of nitrogen and brought into conformal contact with poly(N-isopropylacrylamide)

(PIPAAm) (2% high molecular weight, Scientific Polymers) coated 18 or 25 mm glass coverslips for 30 minutes to ensure transfer of the squares (**Fig. 1 step 2**). ECM squares microcontact printed on PDMS coverslips were used as controls. Upon stamp removal, laser scanning confocal microscopy was used to determine the quality of the transferred ECM squares (Nikon AZ100).

Bovine corneal endothelial cell culture:

Bovine CE cells were isolated and cultured as previously described.(*30*, *41*) Briefly, corneas were excised from the whole globe (Pel Freez), incubated endothelial side up in a ceramic 12 well spot plate with 400 µL of TrypLE Express for 20 minutes. The cells were then gently scraped from the cornea using a rubber spatula, centrifuged at 1500 RPM for 5 minutes, resuspended in 5mL of culture media (low glucose DMEM with 10% FBS, 1% Pen/Strep/AmphB and 0.5% gentamicin, designated at P0 and cultured in a 50 kPa PDMS coated T-25 flask that was pre-coated with COL4. Fifty whole eyes were received at a time and were used to seed 5 T-25 flasks. Cells were cultured until confluence and split 1:3 until they were used once confluent at P2.

Shrink-wrapping CE CELL µMonolayers in ECM scaffolds:

Patterned coverslips (25mm) were secured with vacuum grease to the bottom of 35 mm petri dishes which were placed on dry block set to 52°C. This resulted in the coverslips reaching (within 30 min) and holding at 40°C. Bovine CE cells were released from the culture flask with TrypLE Express, centrifuged and resuspended at a density of 150,000 cells/mL in 15 mL centrifuge tubes. The tubes were placed in a dry block set at 45 ºC for approximately 5 minutes, or until the cell solution just reached 40 ºC and 2mL of cell suspension was added to each 35 mm dish before it was immediately placed in an incubator (37 ºC, 5 % CO2). Cells were cultured on the squares for 24 hours to allow them to form µMonolayers on the 200 µm squares. After 24

hours, samples were removed from the incubator, rinsed twice in 37 °C media to remove non-adherent single cells, 2 mL of fresh warm media was added, and the sample was allowed to cool to room temperature. Once the temperature decreased < 32 °C the PIPAAm dissolved and released the scaffolds + µMonolayers. The release process was recorded using a Photometrics CoolSnap camera. Following release, the scaffolds + µMonolayers were collected via centrifugation at 1500 rpm for 5 minutes before use in further experiments. CE cells seeded on to PDMS coverslips were used as a control.

Immunostaining of shrink-wrapped CE CELL µMonolayers:

Shrink-wrapped µMonolayers resuspended in PBS containing Ca^{2+} and Mg^{2+} (PBS++) were injected through a small gauge needle onto a glass coverslip and allowed to settle for ~15 minutes before fixation for 15 minutes in 4% paraformaldehyde (PBS++). Samples were gently washed 2 times with PBS++ and incubated with 1:100 dilution of DAPI, 1:100 dilution of mouse anti-ZO-1 antibody (Life Technologies) and 3:200 dilution of AlexaFluor 488. Samples were rinsed 2 times for 5 minutes with PBS++ and incubated with 1:100 dilution of AlexaFluor 555 goat anti-mouse secondary antibody for 2 hours. Samples were rinsed 2 times for 5 minutes with PBS++, mounted on glass slides with Pro-Long Gold Antifade (Life Technologies) and then imaged on a Zeiss LSM 700 confocal microscope.

Viability of shrink-wrapped CE cells µMonolayers post-injection:

After centrifugation, shrink-wrapped µMonolayers or TrypLE Express released single cells were resuspended in 200 µL of growth media, drawn up into a 28G needle, injected into a petri dish and incubated with 2 µM calcein AM and 4 µM EthD-1 (Live/Dead Viability/Cytotoxicity Kit, Life Technologies) in PBS++ for 30 minutes at 37 º C. After 30 minutes, samples were imaged on a Zeiss LSM 700 confocal; 5 images per sample and 3 samples per type were used. The

number of live and dead cells was counted manually using ImageJ's multi-point tool. The number of live cells was divided by the number of total cells to determine the percent viability of both the ECM scaffold wrapped cells and enzymatically released cells. The data was compared using a Student's t-test in SigmaPlot. The same methods were used to test the viability of the cells through a 34G needle to test the smallest needle that could be used. The cells were >90% viable post-injection through the 34G needle but could not be accurately quantified due to the small injection volume (2μL) and inability to differentiate between cells (data not shown).

Seeding of shrink-wrapped CE CELL μMonolayers and single CE cells on stromal mimics:

Self-compressed collagen I films were prepared as previously described to mimic the structure of the underlying stroma.(*41*) Briefly, a 6 mg/mL collagen I gel solution was prepared per manufacturer's instructions and pipetted into 9 mm diameter silicone ring molds on top of glass coverslips. The gels were placed into a humid incubator (37 °C, 5% CO2) for 3 hours to compress under their own weight. The gels were then dried completely in a biohood followed by rehydration in PBS, forming a thin collagen I stromal mimic. Shrink-wrapped CE CELL μMonolayers were seeded onto the films at a 1:1 ratio of stamped coverslip to collagen I film. As a control, CE cells that were cultured in the flasks and enzymatically released using TrypLE Express into a single cell suspension were seeded onto collagen I films. The number of control cells seeded was equal to number of μMonolayer cells seeded in the best-case scenario i.e. that all ECM nano-scaffolds on a sample were completely covered in cells. The average number of cells that occupied the 200 μm square was 30 cells: 30 cells x 1600 squares per stamp, meaning approximately 48,000 cells per sample. Therefore, 50,000 cells per sample were seeded for the controls. At 6 and 24 hours, samples were removed from culture and fixed and stained for the nucleus, ZO-1 (tight junction protein) and F-actin. Briefly, samples were rinsed 2 times in

PBS++, fixed in 4% paraformaldehyde (in PBS++) with 0.05% Triton-X 100 for 15 minutes. Samples were rinsed 2 times for 5 minutes with PBS++ and incubated with 5 drops of NucBlue (Life Technologies) for 10 minutes. Samples were rinsed once with PBS++ and incubated with 1:100 dilution of mouse anti-ZO-1 antibody (Life Technologies) and 3:200 dilution of AlexaFluor 488 or 633 phalloidin for 2 hours. Samples were rinsed 3 times for 5 minutes with PBS++ and incubated with 1:100 dilution of AlexaFluor 555 goat anti-mouse secondary antibody for 2 hours. Samples were rinsed 3 times for 5 minutes with PBS++, mounted on glass slides using Pro-Long Gold Anti-fade and imaged on a Zeiss LSM 700 confocal microscope.

In vitro integration of shrink-wrapped µMonolayers vs single bovine CE cells:

To mimic a low-density aging CE, 25,000 P5 bovine cells were seeded onto the collagen I stromal mimics as described above, until confluent to form the low density monolayers. Shrink-wrapped µMonolayers and single CE cells were prepared as above, labeled with CellTracker Green (Life Technologies) for 30 minutes, centrifuged, diluted to the equivalent of 50,000 cells/sample and injected onto the low density monolayers. Low density monolayers with no cells injected on top served as controls. Samples were rinsed 3 hours post injection to mimic the in vivo procedures and new media was added. Media was changed every two days thereafter. Samples were fixed and stained at days 3, 7 and 14 as described above. A Zeiss LSM700 confocal was used to image 10 random spots on each sample and the cell density was manually counted using the multi-point selection tool in ImageJ to count cell nuclei. The number of nuclei was divided by the image area to obtain the cells/mm^2 per image. The cell density for each sample was determined by averaging the cell densities of each image and the average cell density of each sample type was determined by averaging the cell density of the 3 or 4 samples. The data was compared using a one-way ANOVA on ranks with Tukey's test (day 3) or one-way

ANOVA (days 7 and 14) with Tukey's Test is SigmaPlot. To examine the outgrowth of the shrink-wrapped µMonolayers over time, confocal images centered around and individual shrink-wrapped µMonolayer (day 3 n=33, day 7 n=37, day 14 n=40) were collected and the CellTracker channel was converted into a binary black and white image. The binary images for each sample type were then converted into one Z-stack and analyzed via the Heat Map for Z-stacks plugin (relative without log10) for ImageJ to determine the average pixel density of CellTracker.

Live imaging of in vitro integration of shrink-wrapped bovine CE cells:

For live imaging, the monolayer on the collagen I stromal mimic was first incubated for 30 minutes with CellTracker Orange to differentiate between the existing monolayer and injected cells, which were labeled with CellTracker Green as described above. HEPES buffered Opti-MEM I Reduced Serum Media (Life Technologies) with 10% FBS, 1% Pen/Strep was added to the monolayer and shrink-wrapped µMonolayers that were prepared as described above were injected through a 30G needle on top of the sample. The sample was placed on the Zeiss LSM700 confocal equipped with a temperature chamber set to 37°C for 30 minutes to allow for the cells to settle. Using the Definite Focus system, a time-lapse series of one z-stack was obtained every hour for 48 hours. Videos from the time-lapse images were created using the Imaris Software.

Rabbit CE CELL isolation, culture and shrink-wrapping:

Whole rabbit eyes were received on ice from Pel Freez Biologicals. Corneas were excised from the whole globe, the CE and Descemet's Membrane were manually stripped with forceps and incubated in Dispase (1U/mL, Stem Cell Technologies) for 1.5 hours at 37°C to detach the rabbit CE cells (RCECs) from the Descemet's Membrane. The RCECs were then gently pipetted up and down, diluted in culture media (DMEM/F12, 10% FBS, 0.5% Pen/strep), centrifuged at 1500

RPM for 5 minutes, resuspended in 10 mL of culture media, designated at P0 and cultured COL4 coated T-25 flasks with the equivalent of 15-25 eyes per flask depending on cell yield. RCECs were cultured until confluence and split 1:2 and used in all experiments once confluent at P1 or P2. RCEC µMonolayers were shrink-wrapped as described above with the following modifications: ECM scaffolds (using the same 1 cm x 1cm PDMS stamps) were stamped on to 18mm glass coverslips to avoid having excess seeding area and reduce the number of cells that need to be seeded per sample to still achieve full coverage with ~50,000 cells/sample once confluent. Coverslips were secured via vacuum grease to the bottom of Nunc IVF center well dishes (20mm diameter inner well), cells were resuspended at 150,000 cells/mL and 1mL of RCECs was seeded per sample.

Ex vivo integration of shrink-wrapped rabbit CE cells:

Three whole rabbit eyes were placed cornea up in a 12-well plate. Shrink-wrapped RCEC µMonolayers were prepared as described above. Two samples of µMonolayers per ex vivo eye were prepared and resuspended in 100µL of DMEM/F12. A 30-G insulin syringe was used to draw up the full 100µL, the needle was inserted into the center of the cornea until it was visible in the anterior chamber and 50µL of the suspension was injected. This resulted in the equivalent of 50,000 cells injected into the anterior chamber. The needle was held in place for a few seconds to ensure the media and cells did not come back out of the injection site. The injection was viewed under a stereomicroscope and the pink color of the media filling the anterior chamber was visible, indicating successful injection. The eyes were flipped and incubated cornea down for 3 hours at 37°C, 5% CO_2 in a humidified incubator. After 3 hours, the whole eye was placed in 2% paraformaldehyde (PBS++) at 4 °C for 24 hours. After 24 hours the eye was rinsed in PBS and the cornea was excised and rinsed 3 times for 5 mins. The cornea was then incubated

CE facing down on 1 mL of PBS++ containing 2 drops of NucBlue (Life Technologies), 2:100 dilution of mouse anti-ZO-1 antibody (Life Technologies) and 3:200 dilution of AlexaFluor 488 Phalloidin (Life Technologies) for 2 hours at room temperature. Corneas were then rinsed 3 times for 5 minutes in PBS followed by a 2-hour incubation on 1mL PBS++ with 2:100 dilution of AlexaFluor 555 goat anti-mouse secondary antibody for 2 hours and stored in PBS before imaging on the Zeiss LSM700 confocal.

In vivo injection and integration of shrink-wrapped CE cells:

All experimental procedures were reviewed and approved by the University of Pittsburgh Institutional Animal Care and Use Committee (IACUC) and carried out according to guidelines of the Association for Research in Vision and Ophthalmology Resolution on the Use of Animals in Ophthalmic and Vision Research. For both in vivo experiments, shrink-wrapped RCEC µMonolayers were prepared as described above with one minor modification: cells were labeled with Vybrant DiO 1 day prior to seeding on to the ECM nano-scaffolds by incubating cells in 1mL of media with 5 µL of Vybrant DiO for 30 minutes followed by 3 ten minute rinses with fresh media. An excess number of µMonolayer samples were prepared to ensure there was enough volume for injection. The shrink-wrapped µMonolayers were released as described above and after centrifugation at 1500rpm for 5 min, the shrink-wrapped µMonolayers were resuspended in DMEM/F12 at the equivalent of 100,000 cells per 50 µL injection volume (2 stamped samples per 50 µL).

For the first experiment, control single cells were prepared as described above and resuspended in DMEM/F12 at a density of 100,000 cells in a 50 µL injection volume. Six female New Zealand white rabbits with healthy intact CEs weighing approximately 2.5kg were used for this study. Rabbits were anesthetized with Ketamine (40 mg/kg) and Xylazine (4 mg/kg)

intramuscular injection followed by isoflurane inhalation to keep rabbits under sedation for 3 hours. One rabbit did not survive the anesthetization. Rabbits #1 & 2 were injected in the right eye with 50µL (~100,000 cells) of the single cell suspension. Rabbits #3, 4 and 5 were injected with 50 µL of the shrink-wrapped µMonolayer suspension into the right eye using a 30G needle attached to a 500 µL syringe. A tunnel in the corneal stroma was made for the injecting which prevented cell leakage after injection. Immediately after injection, each rabbit was placed on their side with the injected eye facing down for 3 hours to ensure attachment of the cells. On day 7, rabbits were anesthesized with an intramuscular injection of ketamine (40 mg/kg) and xylazine (4 mg/kg) and then euthanized with of Euthasol solution(1 mg/ 4 lbs) containing (390 mg/mL Sodium Pentobarbitol, 50 mg/mL Phenytoin Sodium) through an ear vein injection. Photographic images were obtained via the Google Pixel 2 camera (Supplemental Fig 3) to document eye clarity and the endothelium was viewed using a Nidek Confoscan 3 (Supplemental Fig 4). Eyes were then immediately enucleated and intravitreally injected with 100 uL 2% paraformaldehyde (PBS++). The whole eye was then immersed in 2% paraformaldehyde (PBS++) and fixed at 4°C for 24 hours. After 24 hours the eye was rinsed in PBS and the cornea was excised and rinsed 3x's for 5 mins. The cornea was then incubated CE facing down on 1mL of PBS++ containing 2 drops of NucBlue (Life Technologies) and 2:100 dilution of mouse anti-ZO-1 antibody (Life Technologies) for 2 hours at room temperature. Corneas were then rinsed 3x's for 5 minutes in PBS followed by 2-hour incubation on 1mL PBS++ with 2:100 dilution of AlexaFluor 555 goat anti-mouse secondary antibody for 2 hours and stored in PBS before imaging on the Zeiss LSM700 confocal or a Nikon FN1 base with an A1R HD MP Confocal module. To quantify the density of the integrated cells, the green cells were manually traced with the freehand selection tool, and the "Measure" function was used to determine the area. The

multi-point selection tool was used to determine the number of nuclei within that area and the density was determined by dividing the number of nuclei by the area. The rectangle tool was used to select control areas, areas of non-green (i.e. non-DiO labeled) cells, elsewhere in the image of similar area. The area and cell number were determined the same way as for the DiO labeled areas and the cell density was calculated by dividing the number of nuclei by the area. The number of control areas per image was matched to the number of DiO labeled areas. An example of this is shown in Supplemental Fig 5. Data from the injected eye of both rabbits was pooled together and the cell density of the areas with green cells were statistically compared to those without SigmaPlot using a student T-test.

For the second experiment, only shrink-wrapped μMonolayers were used to determine if cells would integrate and remain in the CE long-term. Six female New Zealand white rabbits with healthy intact CEs weighing approximately 2.5kg were used for this study. Rabbits were anesthetized as described above. All rabbits were anesthetized and injected with 50 μL of the shrink-wrapped μMonolayer suspension into the right eye. Immediately after injection, each rabbit was placed on their side with the injected eye facing down for 3 hours to ensure attachment of the cells. One rabbit went into tachycardia right at the end of the 3 hours and was revived, however, it suffered brain damage as a result of the amount of time without oxygen. That rabbit was sacrificed 24 hours post-injection and the eye was removed and processed as described above and used to determine if the injection processed had been successful (data not shown). At 14 days (2 rabbits) or 28 days (3 rabbits) post-injection, rabbits were sacrificed (as described above) and photographic images were obtained via the Google Pixel 2 camera (Supplemental Fig 3) to document eye clarity and the endothelium was viewed using a Nidek Confoscan 3 (Supplemental Fig 4). Following imaging, eyes were immediately enucleated and

intravitreally injected with 100 uL 2% paraformaldehyde (PBS++). The whole eye was then immersed in 2 % paraformaldehyde (PBS++) and fixed at 4 °C for 24 hours. After 24 hours the eye was rinsed in PBS and the cornea was excised and rinsed 3x's for 5 mins. The cornea was then incubated CE facing down on 1mL of PBS++ containing 2 drops of NucBlue (Life Technologies) and 2:100 dilution of mouse anti-ZO-1 antibody (Life Technologies) for 2 hours at room temperature. Corneas were then rinsed 3x's for 5 minutes in PBS followed by 2-hour incubation on 1mL PBS++ with 2:100 dilution of AlexaFluor 555 goat anti-mouse secondary antibody for 2 hours and stored in PBS before imaging on the Zeiss LSM700 confocal or a Nikon FN1 base with an A1R HD MP Confocal module. To quantify the cell density, images with DiO labeled cells present were taken (n=10+ images) and images were taken far away in areas where there were no green cells (n=5 images) in each cornea. Because the DiO labeled may have faded over time, in this case the cell density of the entire image was counted using the number of nuclei (counted manually via the multi-point tool with only full nuclei being counted) divided by the area of the image. To statistically compare the data, for each rabbit, the density of the images with green cells was compared to the density of the images with no green cells in SigmaPlot using student T-test.

Supplementary Materials

Movie S1. Release of Shrink-wrapped µMonolayers

Movie S2. Time-lapse In Vitro Integration of Shrink-wrapped µMonolayers (Top-down view)

Movie S3. Time-lapse In Vitro Integration of Shrink-wrapped µMonolayers (Side view)

Figure S1. AFM showing nanostructure and height of the patterned ECM nanoscaffolds.

Figure S2. Schematic showing the ex vivo experimental setup.

Figure S3. Rabbit eye photographs.

Figure S4. Confoscan showing normal cobblestone morphology of corneas post injection at 1 and 4 weeks.

Figure S5. Examples of equivalent areas used for Native Cell Density calculations.

Figure S6. Large area Tile-scans of In Vivo Corneas 1 week Post-Injection.

Figure S7. Cell density of areas with green DiO labeled cells compared to areas with no labeled cells

References and Notes:

1. Health Resources & Services Administration, Organ Donation Statistics (2021), (available at https://www.organdonor.gov/statistics-stories/statistics.html).

2. R. Beyar, Challenges in Organ Transplantation. *Rambam Maimonides Med. J.* **2** (2011), doi:10.5041/RMMJ.10049.

3. R. Wu, X. Hu, J. Wang, Concise Review: Optimized Strategies for Stem Cell-Based Therapy in Myocardial Repair: Clinical Translatability and Potential Limitation. *Stem Cells*. **36**, 482–500 (2018).

4. B. J. Hering, W. R. Clarke, N. D. Bridges, T. L. Eggerman, R. Alejandro, M. D. Bellin, K. Chaloner, C. W. Czarniecki, J. S. Goldstein, L. G. Hunsicker, D. B. Kaufman, O. Korsgren, C. P. Larsen, X. Luo, J. F. Markmann, A. Naji, J. Oberholzer, A. M. Posselt, M. R. Rickels, C. Ricordi, M. A. Robien, P. A. Senior, A. M. J. Shapiro, P. G. Stock, N. A. Turgeon, Phase 3 Trial of Transplantation of Human Islets in Type 1 Diabetes Complicated by Severe Hypoglycemia. *Diabetes Care*. **39**, 1230–1240 (2016).

5. A. M. Shapiro, J. R. Lakey, E. A. Ryan, G. S. Korbutt, E. Toth, G. L. Warnock, N. M. Kneteman, R. V Rajotte, Islet transplantation in seven patients with type 1 diabetes mellitus using a glucocorticoid-free immunosuppressive regimen. *N. Engl. J. Med.* **343**, 230–8 (2000).

6. S. Kinoshita, N. Koizumi, M. Ueno, N. Okumura, K. Imai, H. Tanaka, Y. Yamamoto, T. Nakamura, T. Inatomi, J. Bush, M. Toda, M. Hagiya, I. Yokota, S. Teramukai, C. Sotozono, J. Hamuro, Injection of cultured cells with a ROCK inhibitor for bullous keratopathy. *N. Engl. J. Med.* **378**, 995–1003 (2018).

7. K. M. Miah, S. C. Hyde, D. R. Gill, Emerging gene therapies for cystic fibrosis. *Expert Rev. Respir. Med.* **13**, 709–725 (2019).

8. R. Loi, T. Beckett, K. K. Goncz, B. T. Suratt, D. J. Weiss, Limited restoration of cystic fibrosis lung epithelium in vivo with adult bone marrow-derived cells. *Am. J. Respir. Crit. Care Med.* (2006), doi:10.1164/rccm.200502-309OC.

9. C. M. Madl, S. C. Heilshorn, H. M. Blau, Bioengineering strategies to accelerate stem cell therapeutics. *Nature*. **557**, 335–342 (2018).

10. O. Levy, R. Kuai, E. M. J. Siren, D. Bhere, Y. Milton, N. Nissar, M. De Biasio, M. Heinelt, B. Reeve, R. Abdi, M. Alturki, M. Fallatah, A. Almalik, A. H. Alhasan, K. Shah, J. M. Karp, Shattering barriers toward clinically meaningful MSC therapies. *Sci. Adv.* **6**, eaba6884 (2020).

11. H. Abou-Saleh, F. A. Zouein, A. El-Yazbi, D. Sanoudou, C. Raynaud, C. Rao, G. Pintus, H. Dehaini, A. H. Eid, The march of pluripotent stem cells in cardiovascular regenerative medicine. *Stem Cell Res. Ther.* **9**, 201 (2018).

12. M. H. Amer, F. R. A. J. Rose, K. M. Shakesheff, M. Modo, L. J. White, Translational

considerations in injectable cell-based therapeutics for neurological applications: concepts, progress and challenges. *npj Regen. Med.* **2** (2017), doi:10.1038/s41536-017-0028-x.

13. A. A. Foster, L. M. Marquardt, S. C. Heilshorn, The diverse roles of hydrogel mechanics in injectable stem cell transplantation. *Curr. Opin. Chem. Eng.* **15**, 15–23 (2017).
14. EBAA, 2019 EYE BANKING STATISTICAL REPORT 2019 Analysis of Surgical Use and Indications for Corneal Transplant, 775–4999 (2020).
15. N. Joyce, Proliferative capacity of the corneal endothelium. *Prog. Retin. Eye Res.* **22**, 359–389 (2003).
16. C. Zhu, N. C. Joyce, Proliferative Response of Corneal Endothelial Cells from Young and Older Donors. *Investig. Opthalmology Vis. Sci.* **45**, 1743 (2004).
17. N. C. Joyce, B. Meklir, S. J. Joyce, J. D. Zieske, Cell cycle protein expression and proliferative status in human corneal cells. *Invest. Ophthalmol. Vis. Sci.* **37**, 645–55 (1996).
18. N. C. Joyce, S. E. Navon, S. Roy, J. D. Zieske, Expression of cell cycle-associated proteins in human and rabbit corneal endothelium in situ. *Invest. Ophthalmol. Vis. Sci.* **37**, 1566–75 (1996).
19. K. Engelmann, J. Bednarz, M. Valtink, Prospects for endothelial transplantation. *Exp. Eye Res.* **78**, 573–578 (2004).
20. S. Mishima, Clinical Investigations on the Corneal Endothelium. *Am. J. Ophthalmol.* **93**, 1–29 (1982).
21. M. O. Price, P. Gupta, J. Lass, F. W. Price, EK (DLEK, DSEK, DMEK): New Frontier in Cornea Surgery. *Annu. Rev. Vis. Sci.* **3**, 69–90 (2017).
22. I. Dapena, L. Ham, G. R. Melles, Endothelial keratoplasty: DSEK/DSAEK or DMEK - the thinner the better? *Curr. Opin. Ophthalmol.* **20**, 299–307 (2009).
23. A. Anshu, M. O. Price, F. W. Price, Risk of Corneal Transplant Rejection Significantly Reduced with Descemet's Membrane Endothelial Keratoplasty. *Ophthalmology*. **119**, 536–540 (2012).
24. R. N. Palchesko, J. M. Szymanski, A. Sahu, A. W. Feinberg, Shrink wrapping cells in a defined extracellular matrix to modulate the chemo-mechanical microenvironment. *Cell. Mol. Bioeng.* **7**, 355–368 (2014).
25. A. W. Feinberg, K. K. Parker, Surface-initiated assembly of protein nanofabrics. *Nano Lett.* **10**, 2184–2191 (2010).
26. P. W. Alford, A. P. Nesmith, J. N. Seywerd, A. Grosberg, K. K. Parker, Vascular smooth muscle contractility depends on cell shape. *Integr. Biol.* **3**, 1063–1070 (2011).
27. C. S. Chen, M. Mrksich, S. Huang, G. M. Whitesides, D. E. Ingber, Geometric control of cell life and death. *Science (80-.).* (1997), doi:10.1126/science.276.5317.1425.
28. Y. Sun, R. Duffy, A. Lee, A. W. Feinberg, Optimizing the structure and contractility of engineered skeletal muscle thin films. *Acta Biomater.* **9**, 7885–7894 (2013).

29. A. W. Feinberg, W. R. Wilkerson, C. A. Seegert, A. L. Gibson, L. Hoipkemeier-Wilson, A. B. Brennan, Systematic variation of microtopography, surface chemistry and elastic modulus and the state dependent effect on endothelial cell alignment. *J. Biomed. Mater. Res. Part A*. **86A**, 522–534 (2008).

30. R. N. Palchesko, K. L. Lathrop, J. L. Funderburgh, A. W. Feinberg, In Vitro Expansion of Corneal Endothelial Cells on Biomimetic Substrates. *Sci. Rep.* **5**, 32–34 (2015).

31. N. Okumura, Y. Sakamoto, K. Fujii, J. Kitano, S. Nakano, Y. Tsujimoto, S. I. Nakamura, M. Ueno, M. Hagiya, J. Hamuro, A. Matsuyama, S. Suzuki, T. Shiina, S. Kinoshita, N. Koizumi, Rho kinase inhibitor enables cell-based therapy for corneal endothelial dysfunction. *Sci. Rep.* **6**, 1–11 (2016).

32. N. Okumura, N. Koizumi, M. Ueno, Y. Sakamoto, H. Takahashi, H. Tsuchiya, J. Hamuro, S. Kinoshita, ROCK inhibitor converts corneal endothelial cells into a phenotype capable of regenerating in vivo endothelial tissue. *Am. J. Pathol.* **181**, 268–277 (2012).

33. G. Peyret, R. Mueller, J. D'Alessandro, S. Begnaud, P. Marcq, R.-M. Mège, J. M. Yeomans, A. Doostmohammadi, B. Ladoux, Sustained Oscillations of Epithelial Cell Sheets. *Biophys. J.* **117**, 464–478 (2019).

34. M. Deforet, V. Hakim, H. G. Yevick, G. Duclos, P. Silberzan, Emergence of collective modes and tri-dimensional structures from epithelial confinement. *Nat. Commun.* **5**, 3747 (2014).

35. L. M. Marquardt, S. C. Heilshorn, Design of Injectable Materials to Improve Stem Cell Transplantation. *Curr. Stem Cell Reports*. **2**, 207–220 (2016).

36. J. A. Burdick, R. L. Mauck, S. Gerecht, To Serve and Protect: Hydrogels to Improve Stem Cell-Based Therapies. *Cell Stem Cell*. **18**, 13–15 (2016).

37. L. Li, X. Chen, W. E. Wang, C. Zeng, How to Improve the Survival of Transplanted Mesenchymal Stem Cell in Ischemic Heart? *Stem Cells Int.* **2016**, 1–14 (2016).

38. K. Rolev, P. Coussons, L. King, M. Rajan, Experimental models of corneal endothelial cell therapy and translational challenges to clinical practice. *Exp. Eye Res.* **188**, 107794 (2019).

39. C. Murphy, J. Alvarado, R. Juster, M. Maglio, Prenatal and postnatal cellularity of the human corneal endothelium. A quantitative histologic study. *Invest. Ophthalmol. Vis. Sci.* **25**, 312–22 (1984).

40. P. Nucci, R. Brancato, M. B. Mets, S. K. Shevell, Normal endothelial cell density range in childhood. *Arch. Ophthalmol. (Chicago, Ill. 1960)*. **108**, 247–8 (1990).

41. R. N. Palchesko, J. L. Funderburgh, A. W. Feinberg, Engineered Basement Membranes for Regenerating the Corneal Endothelium. *Adv. Healthc. Mater.* **5**, 2942–2950 (2016).

Acknowledgments:

Funding: NIH Grants: NEI 5R01EY024642-04 and NHLBI 5R21HL144235-02

Author contributions: RP completed all in vitro and ex vivo experiments, prepped all of thecells for and observed the in vivo studies, completed all data analysis, prepared all the

figures, and prepared the manuscript. YD performed the injections for the in vivo experiments, gave feedback on data and figures, and editing of the manuscript. MG did all rabbit anesthesization and oversaw all in vivo rabbit experiments and care as well as did all rabbit experiment post-prep and enucleation. SC assisted with rabbit eye dissection for cell retrieval. DS acquired the multi-photon images of the rabbit corneas for in vivo experiments. IK assisted with rabbit experiments. JF and AW oversaw the entire study, gave feedback on data and figures and editing/preparation of the manuscript.

Competing interests: Authors R. Palchesko and A.W. Feinberg are co-inventors on US Patent application No. 20170342374 entitled Extracellular Matrix Scaffolds

Data and materials availability:

Figures:

Movie S1. **Release of Shrink-wrapped µMonolayers.** A time-lapse video showing the release of the shrink-wrapped µMonolayers. Warm PBS with calcium and magnesium was added to the sample and as the temperature decreases below the LCST of PIPAAm, it dissolves, resulting in the release and shrink-wrapping of the µMonolayers.

Movie S2. Time-lapse In Vitro Integration of Shrink-wrapped µMonolayers (Top-down view). This is a time-lapse confocal microscopy video from the top-down view showing the integration of the shrink-wrapped µMonolayers (labeled with CellTracker Green) into an existing monolayer of CE cells (labeled with CellTracker Orange, appearing RED). The micropatterned ECM used to shrink-wrap the µMonolayers is shown in purple.

Movie S3. Time-lapse In Vitro Integration of Shrink-wrapped µMonolayers (Side view). This is a time-lapse confocal microscopy video rendered from the side view showing the integration of the shrink-wrapped µMonolayers (labeled with CellTracker Green) into an existing monolayer of CE cells (labeled with CellTracker Orange, appearing RED). The micropatterned ECM used to shrink-wrap the µMonolayers is shown in purple.